Determination of the Conformation of Molecular Complexes of the Aridicin Aglycon with Ac_2-L-Lys-D-Ala-D-Ala and Ac-L-Ala-γ-D-Gln-L-Lys(Ac)-D-Ala-D-Ala: An Application of Nuclear Magnetic Resonance Spectroscopy and Distance Geometry in the Modeling of Peptides

Luciano Mueller,* Sarah L. Heald, Judith C. Hempel, and Peter W. Jeffs*,†

Contribution from the Department of Physical & Structural Chemistry, Smith Kline & French Laboratories, 709 Swedeland Road, L940, Swedeland, Pennsylvania 19479.
Received May 2, 1988

Abstract: Several 2D nuclear magnetic resonance experiments, including a $^1H-^{15}N$ shift correlation experiment, were used with molecular modeling to define the conformations of molecular complexes of the aglycon of the antibiotic aridicin A (**1**) bound either to the tripeptide Ac_2-Lys-D-Ala-D-Ala (**2**) or to the pentapeptide Ac-L-Ala-γ-D-Gln-L-Lys(Ac)-D-Ala-D-Ala (**3**). The tri- and pentapeptides are bacterial cell-wall fragments, and a goal of this study was to establish whether binding to the tripeptide fragment is sufficient to model the proposed mechanism of action of the antibiotic at the molecular level. Two-dimensional NOE studies of the molecular complexes of the aglycon with **2** and **3** yield the same proton-proton distance constraints for the aglycon and the D-alanyl-D-alanine-L-lysine segment of the bound peptides. Distance geometry was used to generate a solution conformation model for this region of the molecular complexes that is consistent with over 100 NOE derived distances. The N-terminus regions of the bound peptides that do not show NOE interactions with the aglycon have been modeled while the conformation of the core of the molecular complex is held fixed. NOE-derived distance constraints were analyzed to predict conformational characteristics of the solution conformation model. The predictions are supported by an analysis of the core region generated from seven independent distance geometry embedded structures.

Vancomycin-ristocetin class glycopeptide antibiotics are believed to exert their antibiotic activity by binding to bacterial cell-wall precursors that terminate in D-alanyl-D-alanine.[3] These antibiotics are characterized by a central heptapeptide core with a generalized structure shown in Figure 1. The amino acid units G and F are variable and, although the amino acid fragments A-E are highly conserved, they vary in the number and location of chlorine substituents and in the presence or absence of a hydroxyl at C-1′.[4] The crystal structure of a degradation product of vancomycin (CDP-1) has been reported,[5] but the antibiotics as a class are difficult to crystallize. Two-dimensional NMR studies and computer modeling were used previously to define a solution conformation for the aglycon of arridicin A[4d] and the molecular complex of the aglycon of ristocetin bound to Ac_2-L-Lys-D-Ala-D-Ala, a tripeptide in which the α- and ε-amino functions of the lysine side chain are acetylated.[6]

One of our interests was to make a comparison between structural aspects of the binding of the tripeptide (**2**) and the pentapeptide (**3**) to aridicin aglycon. In the past, most of the studies directed to seeking an understanding of the mechanism of inhibition of bacterial cell-wall biosynthesis by glycopeptide antibiotics at the molecular level by NMR methods have involved model studies with the antibiotics or their aglycons with Ac-D-Ala-D-Ala or the tripeptide (**2**). We were interested in exploring the validity of the models obtained from these two peptides by taking an even larger cell-wall fragment, namely the pentapeptide Ac-L-Lys-γ-D-Gln-L-Lys(Ac)-D-Ala-D-Ala. In bacterial cell walls of gram-positive bacteria, this pentapeptide is commonly attached to peptidoglycan precursors at the *N*-acetylmuramic acid residue. Therefore, it was postulated that the pentapeptide might represent a better model to investigate the detailed structural features of binding exhibited by these antibiotics.

In this report, nuclear magnetic resonance studies and molecular modeling are used to define the solution conformation of the aglycon of aridicin A (**1**) bound to Ac_2-L-Lys-D-Ala-D-Ala (**2**) and to the pentapeptide Ac-L-Ala-γ-D-Gln-L-Lys-D-Ala-D-Ala (**3**) consistent with all interproton distances derived from NOE data.

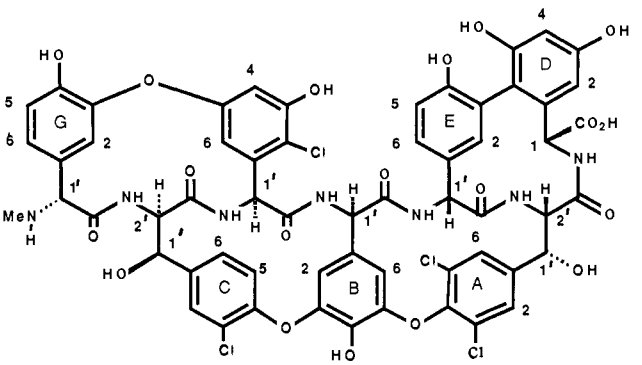

1

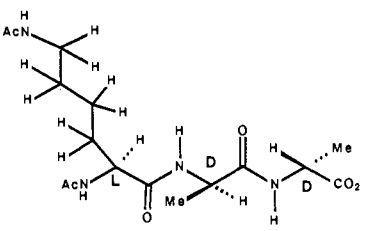

2 Di-N-Acetyl-L-LYS-D-ALA-D-ALA

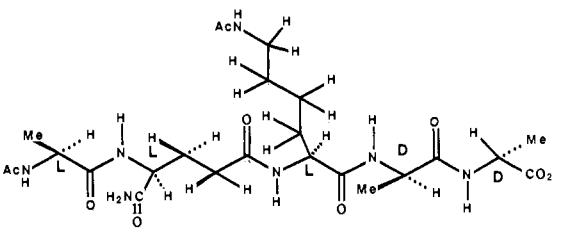

3 L-ALA-γ-D-GLYN-L-LYS-(Ac)-D-ALA-D-ALA

Two-dimensional NOE studies yield the same set of proton-proton distance constraints for the aglycon and the D-alanyl-D-alanine

† Present address: Glaxo Inc., 5 Moore Dr., Research Triangle Park, NC 27709.

0002-7863/89/1511-0496$01.50/0

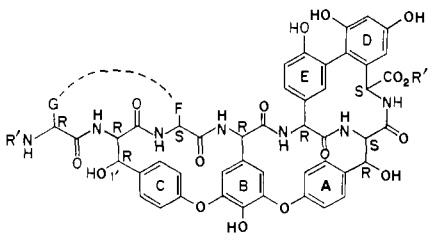

Figure 1. Generalized structure representing the heptapeptide core region of glycopeptide antibiotics of the vancomycin class.

segment of the bound peptide for both molecular complexes studied. Distance geometry[1,2] was used to define a solution conformation model for this region of the molecular complexes that is consistent with over 100 NOE derived distances. This modeling study demonstrates it is possible to generate easily well-built models of cyclic molecules and molecular complexes with distance geometry.

The solution conformation model proposed for the molecular complexes of the aglycon of aridicin A is compared with the solution conformation structure previously proposed for the uncomplexed aglycon,[4d] the common structural elements of the crystal structure of CDP-1, and the solution conformation of the aglycon of ristocetin when bound to the tripeptide Ac_2-L-Lys-D-Ala-D-Ala.[6]

Experimental Section

Sample Preparation. An inoculation of *Kibdelosporangium aridum* (SK&F AAD-216) was made into 20 100-mL flasks containing the seed medium 13H.[12,13] The seed culture was incubated at 28 °C on a shaker at 250 rpm. After 4 days, each of the 20 seed cultures were divided into ≃10-mL aliquots and washed three times with sterile normal saline. The contents of each flask were combined, and the resulting solution was distributed to five centrifuge flasks, centrifuged three times with 45 mL of normal saline, and then reconstituted in normal saline (400 mL). The cell mass from these five flasks was combined, and 40% glycerol (200 mL) was added. The contents were transferred to a fermentor (New Brunswick) containing 8 L of MBSM-2 medium [$MgCl_2CH_2O$, 250 mg/L; $CaCl_22H_2O$, 100 mg/L; NaCl, 1 g/L; $(^{15}NH_4)_2SO_4$, 100 mg/L].[13]

The fermentor was maintained at 28 °C with agitation at 500 rpm and aeration at 4 L/min. Samples were removed daily and analyzed by HPLC, and cells were harvested after 7 days and processed to give the aridicin complex as previously described.[13] The complex was hydrolyzed to give aridicin aglycon, which was purified by preparative HPLC[14,15] to give material for the NMR studies.

The tripeptide Ac_2-Lys-D-Ala-D-Ala and pentapeptide Ac-L-Ala-γ-D-Gln-L-Lys(Ac)-D-Ala-D-Ala were obtained from Sigma.

^{1}H NMR. Two parallel series of experiments in H_2O–DMSO-d_6 and D_2O–DMSO-d_6 were performed for the complexes of the aridicin aglycon with the tripeptide or pentapeptide. Data collection was done on a JEOL GX500 spectrometer operating at 500.13-MHz proton frequency. All two-dimensional spectra were calculated and analyzed on a VAX 11/785 with D. Hare's FTNMR software.[7] COSY data were collected with the standard two-pulse sequence and presented as magnitude spectra. Double-quantum spectra were obtained as described previously.[4d] Experiments in D_2O solution were performed with a spectral width of 5000 Hz. In H_2O solutions the spectral width was increased to 7002 Hz to capture the amide resonance of CNH. Phase-sensitive NOESY experiments were collected with mixing times of 200, 300, and 400 ms. Experiments were done at 25 or 17 °C. Water suppression in H_2O solution was normally achieved by presaturation. However, some NOESY experiments were obtained with the following alternate pulse sequence, which did not require any presaturation of the solvent peak:

$$90°\text{–}t_1\text{–}90°\text{–}\tau_m\text{–HS–}\tau_r\text{–}(1331)_{HORE}\text{–acquire–}R\text{–delay}$$

A similar sequence has been previously suggested by Schwartz et al.[8] and was later modified by Pardi and co-workers.[18] We find that our sequence, which employs a 1.5-ms homogeneity spoiling pulse near the end of the mixing period, yielded the best results. The use of the HORE pulse requires large linear phase shifts across the spectrum, which on the JEOL system creates large base-line rolls due to slow response time of the low-pass filters in the GX receiver. This effect is overcome by the use of a polynomial base-line correction in both frequency domains of the NOESY spectra. The homonuclear mixing experiment was performed with a mixing period of 53 ms by the MLEV-17 sequence.[9] The radio frequency field strength was set to 12.5 kHz, and the solvent peak was suppressed by presaturation.

All two-dimensional experiments were acquired with 512 t_1 values with the exception of the MLEV-17 experiment where only 256 t_1 FIDs were collected. In the magnitude COSY spectra, a 10°-shifted sine bell was used prior to Fourier transformation, whereas in the phase-sensitive spectra, a 90°-shifted sine bell was employed. Appropriate zero-filling was employed in all 2D spectra to yield 1K × 1K spectra. The NOESY spectra were improved considerably by polynomial base-line correction in both dimensions. The volume integral of NOESY cross peaks were computed over a square area of 24 Hz with the "i" command in FTNMR version 4.5. Distances were estimated by reference to the proton pairs C6, C5 and G6, G5. In the NOESY spectra obtained with the HORE acquisition pulse, the amplitude modulation along the F_2 axis was taken into account by using a series of different distance markers across the spectrum, i.e., cross peak C6, C5 in region 1, C5, C6 in region 2, and G5, G6 in region 3.

To compensate for the effects of spin diffusion, we generated asymmetric bounds in the input file to the distance geometry program. For distances less than 3 Å, upper and lower bounds were set to ±0.25 Å. For distances between 3 and 3.5 Å, the upper bounds were increased to +0.3 Å, whereas the lower bounds remained the same as defined above. For distances greater than 3.5 Å, upper bounds were set to +0.6 Å and lower bounds to −0.4 Å. The very good match between asymmetric bounds and distances derived from structures built with distance geometry provides support for this simple approach (vide infra).

^{15}N NMR. All ^{15}N shifts were observed indirectly using proton-observed detection of proton–nitrogen zero- and double-quantum transitions. Most of the data collection was carried out with the recently developed constant-time method called POWERSPIN.[10] A delay of 20.5 ms was employed. When the echo pulse is moved, 64 t_1 FIDs were recorded per two-dimensional experiment, with each FID consisting of a sum of 256 scans. The spectral width was 1600 Hz in the indirectly detected nitrogen frequency domain and 3201 Hz in the proton frequency domain. The proton pulses were 1331 REDFIELD pulses with the carrier frequency centered in the amide resonance region in order to suppress the large water peaks (the solvent was a 1:1 mixture of DMSO-d_6 and H_2O). The experiments on the mixtures containing the tripeptide were performed on a JEOL GX400 spectrometer, which was equipped with a special proton-observed ^{15}N probe in the laboratory of Dr. Stanley Opella

(1) Havel, T. F.; Kuntz, I. D.; Crippen, G. M. *Bull. Math. Biol.* **1983**, *45*, 665–720.
(2) Crippen, G. M.; Havel, T. F. *Acta Crystallogr.* **1978**, *34*, 282–284.
(3) (a) Reynolds, P. E. *Biochim. Biophys. Acta* **1961**, *52*, 403–405. (b) Jordan, D. C. *Biochem. Biophys. Res. Commun.* **1961**, *6*, 167–170. (c) Perkins, H. R. *Biochem. J.* **1969**, *111*, 195–205.
(4) (a) Harris, C. M.; Harris, T. M. *J. Am. Chem. Soc.* **1982**, *104*, 363–365. (b) Hunt, A. H.; Dorman, D. E.; DeBono, M.; Mallory, R. M. *J. Org. Chem.* **1985**, *50*, 2031–2035. (c) Bana, J. C. J.; Williams, D. H.; Stone, D. J. M.; Leung, T.-W. C.; Doddrell, D. M. *J. Am. Chem. Soc.* **1984**, *106*, 4895–4902. (d) Jeffs, P. W.; Mueller, L.; DeBrosse, C.; Heald, S. L.; Fisher, R. *J. Am. Chem. Soc.* **1986**, *108*, 3063–3075.
(5) Sheldrick, G. M.; Jones, P. G.; Kennard, O.; Williams, D. H.; Smith, G. A. *Nature (London)* **1978**, *271*, 223.
(6) Fesik, S. W.; O'Donnell, T. J.; Gampe, R. T.; Olejniczak, E. T. *J. Am. Chem. Soc.* **1986**, *108*, 3165–3170.
(7) Hare, D. R., Hare Research, Inc., 14810 216th Ave., NW, Woodinville, WA 98072.
(8) Schwartz, A. L.; Cutnell, J. D. *J. Magn. Reson.* **1983**, *53*, 398.
(9) Davis, D. G.; Bax, A. *J. Am. Chem. Soc.* **1985**, *107*, 2820–2821.
(10) Mueller, L.; Schiksnis, R. A.; Opella, S. *J. Magn. Reson.* **1986**, *66*, 379–384.
(11) Wianowski, M.; Stefaniak, L.; Webb, G. A. *Annu. Rep. NMR Spectrosc.* **1981**, *11*, 1–494.
(12) Shearer, M. C.; Actor, P.; Bowie, B. A.; Grappel, S. F.; Nash, C. H.; Newman, D. J.; Oh, Y. K.; Pan, C. H.; Nisbet, L. J. *J. Antibiot.* **1985**, *38*, 555–560.
(13) Chung, S. K.; Taylor, P.; Oh, Y. K.; DeBrosse, C.; Jeffs, P. W. *J. Antibiot.* **1986**, *39*, 642–651.
(14) Sitrin, R. D.; Chan, G. W.; Dingerdissen, J. J.; Holl, W.; Hoover, J. R. G.; Valenta, J. R.; Webb, L.; Snader, K. M. *J. Antibiot.* **1985**, *38*, 561–571.
(15) Sitrin, R. D.; Chan, G. W.; Chapin, F.; Giovenella, A. J.; Grappel, S. F.; Jeffs, P. W.; Phillips, L.; Snader, K. M.; Nisbet, L. J. *J. Antibiot.* **1986**, *39*, 68–75.
(16) (a) Kalman, J. R.; Williams, D. H. *J. Am. Chem. Soc.* **1980**, *102*, 906–912. (b) Convert, O.; Bongini, A.; Feeney, J. *J. Chem. Soc., Perkins Trans. 2*, **1980**, 1262–1270. (c) Fesik, S. W.; Armitage, I. M.; Ellestad, G. A.; McGahren, W. J. *Mol. Pharmacol.* **1984**, *25*, 281–286.
(17) Jeener, J.; Meier, B. H.; Bachmann, P.; Ernst, R. R. *J. Chem. Phys.* **1979**, *71*, 4546–4552.
(18) Bach, A. C.; Selsted, M. E.; Pardi, A. *Biochemistry* **1987**, *26*, 4389–4397.

at the University of Pennsylvania. The experiments involving the pentapeptide were performed in our laboratory on a JEOL GX500 spectrometer operating at 500-MHz proton frequency. Again, these experiments were performed on a special proton-observed ^{15}N probe. This probe had a proton sensitivity of 230:1 in 0.1% ethylbenzene.

The nitrogen chemical shifts were referenced externally to nitromethane (a sealed capillary containing neat ^{15}N-enriched nitromethane was purchased from Stohler Isotopes). The nitromethane nitrogen shift was measured as follows: The concentric tube containing neat nitromethane was immersed in a 1:1 mixture of DMSO-d_6 and H_2O containing 0.1 M of ^{15}N-enriched *N*-acetylglycine inside a 5-mm NMR tube. Corrections for bulk susceptibility were made with the equation of Wianowski.[11] The susceptibility of the DMSO–H_2O mixture was assumed to be the mean of the susceptibilities of the corresponding neat solvents. This gave a susceptibility of -0.667×10^{-6} for our solvent. This led to a ^{15}N shift correction term of −1.29 ppm. The tabulated shifts are given relative to neat ammonia, assuming a chemical shift for nitromethane of 380.23 ppm. Most ^{15}N experiments were performed at 30 °C. The concentration of the glycopeptide was 20 mM, with varying amounts of tripeptide or pentapeptide present.

Modeling. Distance geometry[1,2] was used to calculate the core region structure (see Figure 7) of the molecular complexes. The Lys side chain of the bound peptide is represented by $-CH_2CH_3$ in modeling studies of this region of the molecular complexes and the N-terminus of the Lys residue is acetylated. The conformational range of the N-terminus region of the bound peptides was investigated with interactive computer modeling tools implemented in the SYBYL modeling system. Models were investigated in which the binding region of the molecular complex was held fixed and sterically allowed conformations of the N-terminus region of the bound peptides consistent with NOE constraints internal to these regions of the molecular complex were added. NOE studies provide the same distance constraints for the binding region common to both complexes (Table II) within the accuracy of the NMR observations.

The distance geometry algorithm EMBD[1,2] was used to generate conformations that are consistent with bond distances, distances between atoms bonded to a common atom, and the hydrogen–hydrogen distances determined from NOE studies (Table II). Hydrogen-bonding constraints linking the amide hydrogens of the B and C residues of the aglycon with the carboxy terminus of the bound peptide were also specified (Table V). The ^1H and ^{15}N chemical shift changes observed for these amide hydrogens support the hydrogen-bonding assignments. The lower bound for unknown distances between atoms was specified by the sum of their van der Waals radii. The upper bounds for the unknown distances were specified with triangle sum rules, and the upper and lower bounds of the unknown distances were further refined with triangle sum rules.[1,2] This core region was modeled using all atoms plus dummy atoms at the centroids of aromatic rings and methyl groups (a total of 185 atoms).

The planar atoms associated with the aromatic side chains of the aglycon of aridicin A were treated as fused elements in the distance geometry input, sets of atoms for which all interatomic distances are known and specified. Chiral centers were specified[4d] (see structure **1**) along with planarity constraints for aromatic carbons, carbonyl carbons, and amide nitrogens. All peptide bonds were set trans with the exception of the peptide bond linking residues E and D of the aglycon of aridicin A, which was set cis.[4d] The distance geometry algorithm converts a distance matrix representation of a molecular conformation into Cartesian coordinates and refines the Cartesian coordinates against distance, chirality, and planarity constraints.

Seven conformers (labeled a–g) were generated with this set of constraints in seven cycles of the distance geometry algorithm. Distance constraints were used to refine the conformers generated by the EMBD algorithm with the distance constraint error function (eq 1) where d = 0 if the interatomic distance falls inside the bounds specified for that distance otherwise d = difference between the calculated value and the closest bound.

$$\text{error} = \sum d^2 \tag{1}$$

A total of 75 min of CPU time (VAX 11/780) were required to generate and refine each structure against distance, chirality, and planarity constraints. The square root of the distance error function for six of the seven conformers is 1.7 Å or less over the 185 × 185 distance matrix while conformer e is characterized by a value of 2.3 Å. All structures correspond to the desired chiralities with the exception of conformer f in which the β-carbon of the A ring has the wrong chirality relative to the other chiral centers of the molecule.

The conformers were analyzed, as discussed in the Results and Discussion, and selected conformers b and e were refined by energy minimization with MAXIMIN force field parameters and Gaustiger charges (as implemented in version 3.4 of the SYBYL modeling system, registered trademark of Tripos Associates, Clayton, MO). Approximately 5 h of CPU time (VAX 11/780) was required to minimize conformer e and approximately 8 h of CPU time to minimize conformer b.

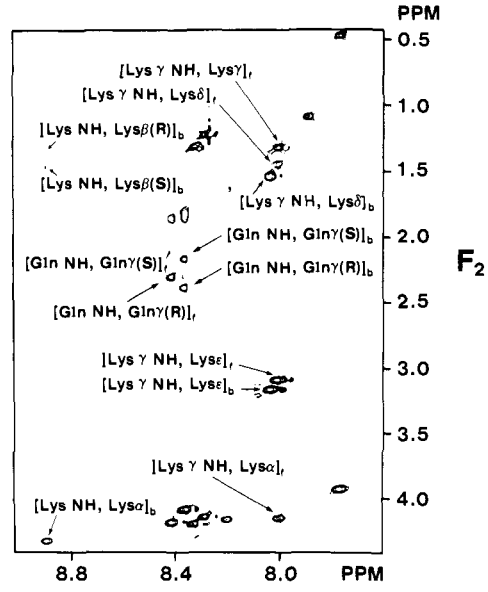

Figure 2. HOHAHA of pentapeptide depicting connectivities from NH resonances to corresponding CH peaks. Cross-peaks are identified within parentheses as b or f corresponding to symbols originating from either the bound or free form of the pentapeptide, respectively.

Results and Discussion

^1H NMR. Assignment of the proton resonances in the complexes formed between aridicin aglycon and Ac_2-L-Lys-D-Ala-D-Ala and the aglycon and Ac-L-Ala-γ-D-Gln-L-Lys(Ac)-D-Ala-D-Ala were obtained with COSY and NOESY experiments. Initial spectra obtained for solutions in D_2O permitted the assignment of most resonances. Connectivities to the amide NH resonances were obtained from spectra acquired in H_2O solutions. Intraresidue connectivities, particularly those involving the NH and the respective side chains of the lysine and glutamine residues in the pentapeptide, were confirmed by homonuclear mixing (HOHAHA) spectra. The results of the HOHAHA experiment for the molecular complex containing the pentapeptide are illustrated in Figure 2. Remote connectivities are observed for all residues in the pentapeptide chain. These cross peaks are seen in both the uncomplexed and complexed forms of the pentapeptide.

Some peptide resonances undergo marked changes in chemical shift upon binding (a complete list of chemical shifts of all observable protons is given in Table I). The largest shift change is exhibited by the methyl protons of the terminal D-alanine residue. Similar shifts have been reported previously for this residue in other glycopeptide complexes of the vancomycin antibiotics.[16] This effect results from the ring current in the B ring experienced by the D-alanine methyl group when bound. Binding also results in dispersion in the chemical shifts between several of the geminal protons in the side chains of the lysine and D-glutamine residues for the pentapeptide. This increased dispersion suggests that the conformation of these two amino acid side chains may be restricted in the complex.

A comparison of the proton chemical shifts (Table I) for the tripeptide and pentapeptide complexes shows a very close match for the C-terminal L-Lys-D-Ala-D-Ala residues in the two complexes in the bound state. A close correspondence also exists in ^{15}N chemical shifts of the C-terminal tripeptide region in both complexes (see Table III). In addition to these similarities in chemical shifts, the NH–CH^{α} J couplings for comparable residues in the tri- and pentapeptide are very similar. An expanded region of the NOESY spectrum of the pentapeptide complex in water acquired with the 1331 HORE pulse is depicted in Figure 3. Strong cross peaks between Ala^5 NH, Ala^4 CH^{α}, Ala^4 NH, and Lys^3 CH^{α} confirm the sheet conformation of the putative cell wall precursor in the binding pocket. Comparison of the results from the NOESY spectra confirms that the L-Lys-D-Ala-D-Ala termini

Table I. Chemical Shifts and Coupling Constants of Aridicin Aglycon–Aglycon Complexes with Tripeptide (**2**) and Pentapeptide (**3**)

	tripeptide complex[a]		pentapeptide complex[a]				tripeptide complex[a]		pentapeptide complex[a]		
proton	shift, δ	*J* coupling, Hz	shift, δ	*J* coupling, Hz		proton	shift, δ	*J* coupling, Hz	shift, δ	*J* coupling, Hz	
CNH	11.83	10.9	11.87	11.1		B6	5.07	s	5.05		
FNH	9.34	10.15	9.36	10.3		G1′	4.91	s	4.92		
BNH	8.92	9.4	8.94	8.4		E1′			4.69		
ENH	8.91	overlapped	8.87	overlapped		Ala^4 C^α	4.56		4.58		bound
Lys^3 NH	8.62	7.8	8.87	7.6	bound	D1′			4.55		
DNH	8.62	6.8	8.48	6.0		A2′			4.42		bound
Gln^2 γ-NH			8.45	8.0	free	Lys^3 C^α	4.30		4.32		bound
Gln^2 γ-NH			8.34	7.8	bound	Ala^4 C^α	4.30		4.20		free
Ala^1 NH			8.35	6.8	free	Ala^5 C^α	4.23		4.15		free
Ala^1 NH			8.25	5.2	bound	Ala^1 C^α			4.20		free
Ala^4 NH	8.30	7.0	8.28	6.8	free	Gln^2 C^α			4.19		free
Lys^3 NH	8.18	6.25	8.22	6.2	free	Lys^3 C^α	4.17		4.16		free
Ala^5 NH	8.15	7.1	7.97		free	Ala^1 C^α			4.15		bound
Lys γ-NH	8.01	6.25	8.03	5.7	bound	Gln^2 C^α			4.07		bound
Lys γ-NH	7.98	5.5	8.06	6.0	free	Ala^5 C^α	3.93		3.93		bound
Ala^4 NH	7.87	7.1	7.87	7.0	bound	Lys^3 C^ϵ	3.16		3.16		bound
Ala^5 NH	7.75	8.4	7.74	8.0	bound	Lys^3 C^ϵ	3.09		3.09		free
E2	7.74	s	7.71			NMe	2.60	s	2.60		
C6	7.64	7.8	7.63			Gln^2 C^γ (*R*)			2.37		bound
A6	7.60	s	7.58			Gln^2 C^γ (*R*)			2.30		free
Gln NH_2[a]			7.56		bound	Gln^2 C^γ (*S*)			2.16		bound
Gln NH_2[a]			7.45		free	Gln^2 C^γ (*S*)			2.09		free
C2	7.24	s	7.24			Gln^2 C^β (*R*,*S*)			1.86		free
Gln NH_2[b]			7.06		bound	Gln^2 C^β (*S*)			1.85		bound
Gln NH_2[b]			7.02		free	Gln^2 C^β (*R*)			1.82		bound
C5	7.12	7.8	7.13			Ala^1 $NHCOCH_3$	1.98	s	1.97		bound
G6	7.05	8.0	7.06			Ala^1 $NHCOCH_3$	1.97	s	1.96		
ANH	7.04	10.0	6.98			Lys^3 $NHCOCH_3$	1.94	s	1.96		bound
A2	7.02	s	6.99			Lys^3 $NHCOCH_3$	1.92	s			
E6	6.86	8.6	6.85			Lys^3 C^β (*R*)	1.69		1.69		free
E5	6.78	8.6	6.78			Lys^3 C^β (*S*)	1.62		1.64		free
G5	6.72	8.0	6.72			Lys^3 C^δ (*R* or *S*)	1.54		1.53		bound
F4	6.71	s	6.72			Lys^3 C^β (*S*)			1.47		bound
G2	6.65	s	6.65			Lys^3 C^δ (*R* or *S*)	1.44		1.45		free
F6	6.48	3.1	6.48			Lys^3 C^γ (*R* or *S*)	1.36		1.34		free
D4	6.39	s	6.34			Ala^5 C^β	1.36	7.0	1.32		free
D2	6.29	s	6.34			Ala^4 C^β	1.30	7.0	1.32		free
F1′	6.21	10.15	6.20	10.5		Ala^1 C^β			1.32		free
B1′	5.69	9.4	5.69	8.9		Lys^3 C^γ (*R* or *S*)	1.30		1.31		bound
B2	5.55	s	5.55			Lys^3 C^β (*R*)			1.30		bound
C2′	5.35	10.2 + 5.5	5.35	10.3 + 5.3		Ala^1 C^β			1.22		bound
C1′	5.28	5.5	5.28	5.3		Ala^4 C^β	1.09		1.09		bound
A1′	5.25	s	5.27			Ala^5 C^β	0.47		0.47		bound

[a] A uniform numbering system is used for the pentapeptide and tripeptide that is based upon that shown for the pentapeptide, e.g. D-Ala^5-D-Ala^4-L-Lys^3-γ-Gln^2-L-Ala^1 and D-Ala^5-D-Ala^4-L-Lys^3.

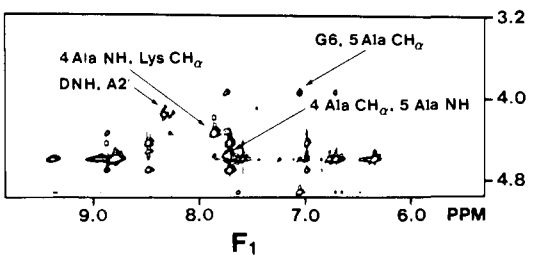

Figure 3. NOESY spectrum of the pentapeptide complex showing region illustrating intrapentapeptide NOE's from β-sheet conformation.

of both peptides have the same conformation in the binding pocket within the accuracy of the NOESY data. A question to be addressed by modeling is whether a conformation or conformations can be built to express all constraints simultaneously.

To minimize effects of spin diffusion, distances were derived only from spectra recorded at mixing times of 200 and 300 ms. Despite this, it is expected some of the longer interproton distances will still be biased to too short values due to spin diffusion. Evidence that this was indeed the case was found in the linear string of closely spaced protons G5, G6, and G1′ in the G residue at the N-terminus of aridicin. The NOESY cross-peak intensity obtained at a mixing time of 200 ms between G1′ and G5 indicates a distance of 3.7 Å whereas the distance between G1′ and G5 is 4.6 Å in well-built molecular models.

Distances over a range from 2.0–4.0 Å obtained from NOE at single mixing times are less accurate than those derived from build-up rates. Nonetheless, when all of the NOESY data in the pentapeptide complex were used, 80 NOE-derived intrapeptide distances were determined for the aglycon and 35 for the pentapeptide. In addition, 35 interpeptide NOE-derived distances were assigned. These data form the basis for our modeling studies. As indicated in the Experimental Section, the extraction of so many NOE distances was made possible by (1) observing NOESY cross peaks from C^α protons that were observed under the water peak through the use of the HORE pulse sequence (see the Experimental Section) and (2) flattening the base plane in the NOESY spectra by polynomial base-line corrections.

A number of NOE distance constraints provided by the NMR data on the aridicin aglycon–pentapeptide complex permitted the stereospecific assignment of the methylene protons in the glutamine side chain and the C^β protons in the lysine residue. For example, the stereochemical differentiation of the *pro-R* and *pro-S* β-protons of the lysine residue is provided by two intrapeptide NOE's, one between the Lys C^β *pro-R* hydrogen and the Ala^4 NH and the other involving Lys C^β *pro-S* hydrogen and the Lys NH. Similarly, the orientation of the isoglutamine side chain is indicated by the observation of much stronger cross peaks from one C^β

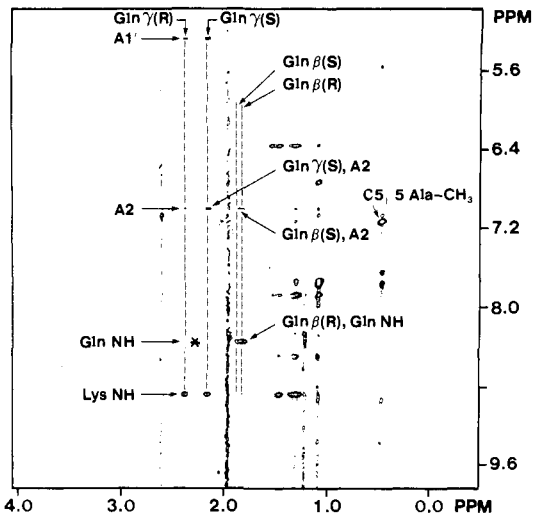

Figure 4. Inter- and intraresidue cross peaks from the diastereotopic methylene protons in the γ-glutamine residue and aridicin aglycon.

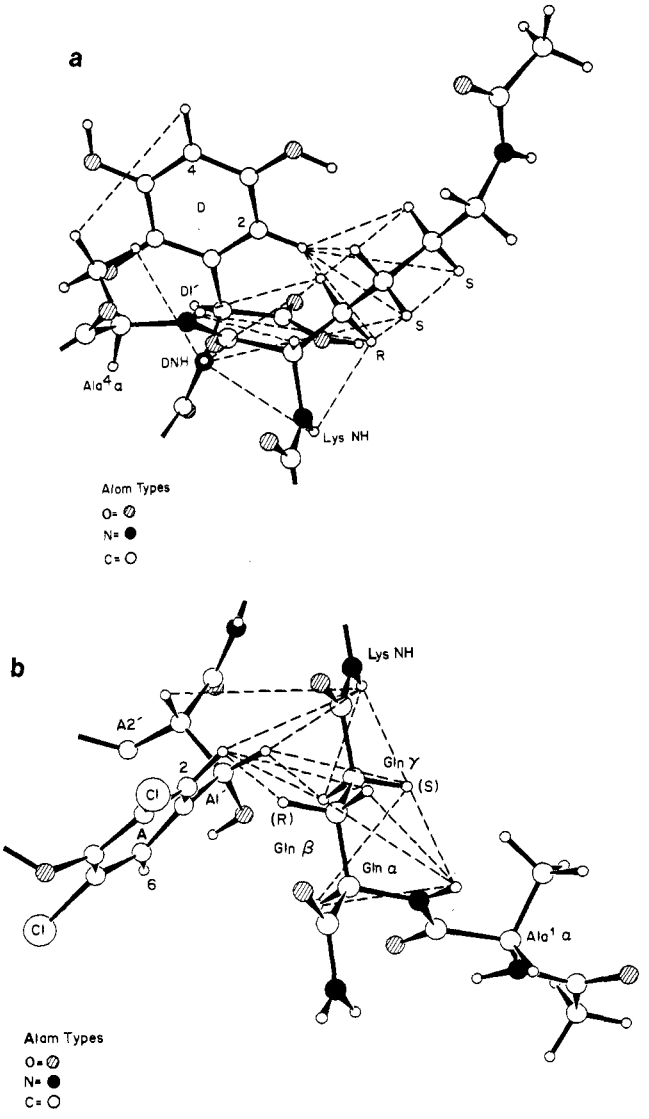

Figure 5. Diagram showing stereochemical disposition of (a) the lysine and (b) γ-glutaminyl side chains relative to the aglycon heptapeptide core. The dotted lines connect pairs of hydrogens that are correlated through NOE-derived distance relationships.

proton and one C^{γ} proton to the A2 and A1′ protons of the aglycon than from the corresponding diastereotopic partners at these positions (see Figure 4). While there may be some ambiguity

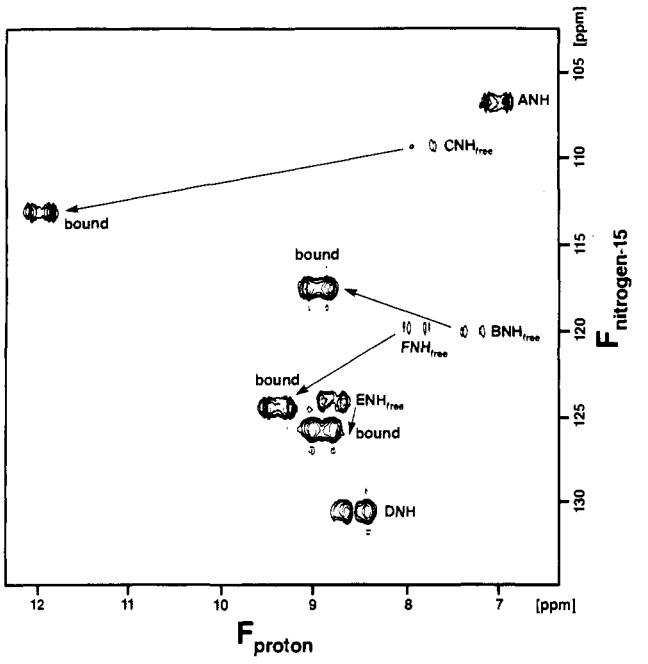

Figure 6. ^{1}H–^{15}N heterocorrelation spectrum of ^{15}N-labeled aridicin aglycon in the presence of excess pentapeptide (3).

in specifying the stereochemical identity of the protons showing the stronger cross peaks to the A2 and A1′ protons, the general conformational features indicated by the intrapeptide NOE's in the isoglutamine residue suggest a fully extended staggered conformation, in which the *pro-S* hydrogens at the C^{β} and C^{γ} positions face into the aglycon nucleus (see Figure 5). As expected, there is a marked increase in motional freedom as one moves toward the N-terminus of the pentapeptide in the complex, as evidenced by decreased intensities of the NOE interactions leading to overexaggeration of the computed distances (based upon the internal C5, C6 and G5, G6 distance standard). This is most evident for distances derived for both the C^{α} and amide NH protons to adjacent residues. Finally, the NOE pattern for the terminal Ala^{1} residue shows the typical profile of a random coil peptide, with all the NOE's exhibiting weak peaks of equal intensity.

^{15}N NMR. The opportunity to exploit the ^{15}N nucleus for extracting structural information for complex molecules suffers from limitations imposed by the isotope's low natural abundance (0.37%), its weak magnetic moment, and negative gyromagnetic ratio. These limitations were obviated by biosynthetic enrichment of the ^{15}N isotope and by employment of indirect detection of the ^{15}N nucleus. The latter experiment was carried out as described by Mueller[19] and involves excitation of heteronuclear multiple-quantum transitions and their detection through the ^{1}H signals. This method overcomes the problems associated with low sensitivity and the negative gyromagnetic ratio.

Biosynthetic incorporation of ^{15}N into aridicin A was readily achieved by administering [^{15}N]ammonium acetate during the logrithmic growth phase to cultures of *K. aridum* grown on chemically defined medium (see the Experimental Section). The level of enrichment was approximately 10% from an estimate made from the intensities of the side bands from the ^{15}N satellites in the proton spectrum. The resulting increase in abundance of the ^{15}N isotopic content of the antibiotic provided material for the NMR studies.

The ^{1}H–^{15}N heterocorrelation experiments with the tripeptide and pentapeptide complexes of the aglycon gave comparable results for corresponding amides. The chemical shift of the three amide nitrogens B, C, and F in the carboxylate binding pocket all undergo chemical shift changes after complexation to the D-Ala terminus of the peptides. (See Table III and Figure 6.) The C and F amide

(19) Mueller, L. *J. Am. Chem. Soc.* **1979**, *101*, 4481–4484.

nitrogen signals shift downfield, with the largest shift exhibited by the F nitrogen. The B nitrogen chemical shift unexpectedly moves upfield in both the tri- and pentapeptide complexes. The chemical shift changes observed for the nitrogen nucleus at these sites are in contrast with those observed for the corresponding protons. The proton chemical shifts all undergo downfield shifts on formation of the complex as expected from the results of analogous studies.[16]

The DNH group, which is situated in a position to permit it to form a hydrogen bond to the carbonyl of the L-lysine residue, does not exhibit any noticeable change in chemical shift of either the ^{15}N or ^{1}H signals upon formation of the complexes. In similar fashion and not unexpectedly, no changes are observed for the shifts of the ANH residue, which is situated on the outer convex face of the aglycon. In contrast, the ENH group, which is also located on the outer convex surface, undergoes a downfield shift on the ^{15}N axis upon formation of either the tripeptide (1.6 ppm) or pentapeptide (1.7 ppm) complex. Since the ENH proton shift is essentially unchanged, the origin of the ^{15}N chemical shift change may be induced through formation of the hydrogen bond between the B-2′ carbonyl residue and the Ala^4 NH. Downfield ^{15}N shifts are observed in peptides irrespective of whether the particular amide group is involved in either accepting or donating a H bond.[20]

We attempted to correlate changes induced in proton chemical shifts with the formation of interpeptide hydrogen bonds in the complexes. The proton shifts were correlated with the empirical equation proposed by Wagner et al.[21] that relates changes in chemical shift upon formation of a hydrogen bond with hydrogen bond distance. The results showed a good correlation for the amide protons in aridicin aglycon with hydrogen bond distances from an energy-refined structure of the aglycon–tripeptide complex. These comparisons are shown in Table IV. The CNH proton, which experiences the largest change in chemical shift, shows the shortest H-bond distance in the model. Overall, there is a very good correlation between calculated and experimental values. From the results discussed above, it is obvious that the ^{15}N shifts exhibit more complex behavior than is shown by proton shifts in systems involving amide–carbonyl hydrogen bonding interactions.[22] An important conclusion derived from the results is that despite the proximity of the DNH and the carbonyl of the D-Ala^4 residue, there is no evidence for a hydrogen bond between these residues in either the tripeptide or pentapeptide complex.

A comparison of the lifetimes of the complexes between aridicin aglycon and the cell-wall peptides was made from the ratio of volume integrals of transferred NOE cross peaks and the corresponding diagonal peaks using the equations described by Jeener et al.[17] At 25 °C the lifetime for the tripeptide complex was 0.29 s and that of the pentapeptide complex was 0.45 s. This suggests that there is increased binding of the pentapeptide to the aglycon compared to that of the tripeptide. The increased lifetime of the pentapeptide complex when compared with the tripeptide complex (0.45 s vs 0.29 s) suggests an increased stability for the former.

Modeling. No information other than distance, chirality,[4d] and planarity constraints derived from the chemical structure and the NMR studies of the complexes was used in the generation of the seven structures that were derived from the modeling studies. The derivation of distance information from the intensities of NOE's obtained at a single mixing time is limited primarily by spin diffusion. This has been referred to earlier in this paper and has been discussed in detail by others.[23] The very good match between input distances with asymmetric NMR bounds and distances derived from structures built with distance geometry provides

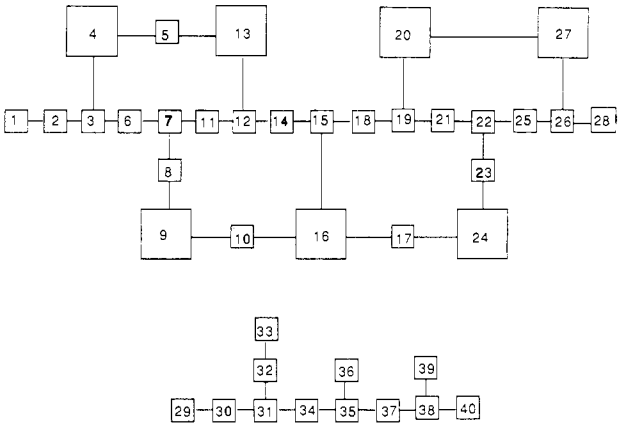

Figure 7. Structural templates for the binding region common to aridicin A aglycon bound to tri- or pentapeptide. The rotatable bonds of the aglycon and tripeptide (Figure 1) are defined by the solid lines that connect boxes representing structural templates. Structural templates associated with hydroxyl substituents are not included. It is proposed that localized and correlated NOE's (Figure 8) restrict the conformational freedom of the rotatable bonds to define conformational domains.

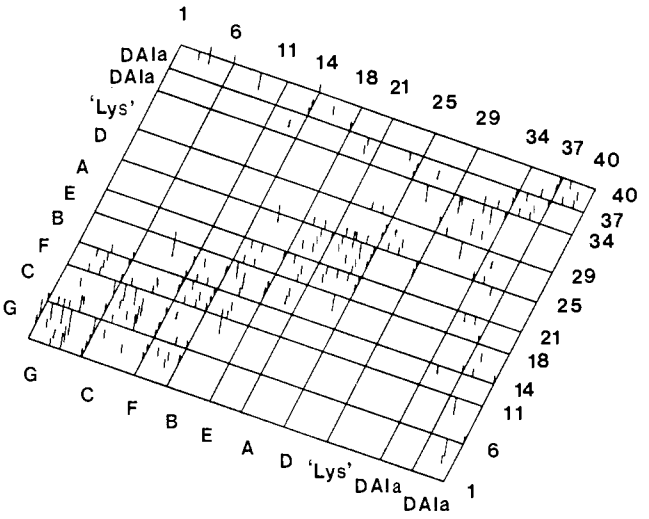

Figure 8. Distribution of NMR distance constraints. Peak heights are proportional to the number of observations linking structural templates. Peptide bond templates are identified by template number. The identity of each block of structural templates is indicated with the one-letter code for the residues of the aglycon (Figure 1) and a three-letter code for the tripeptide.

support for the asymmetric bounds approach. The average deviation over the 107 NMR-derived distance constraints is ≤0.024 Å in all seven models of the aglycon–tripeptide complex. The deviations are discussed in greater detail below.

The rotatable bonds of the binding region of the aglycon and tri- or pentapeptide are illustrated in Figure 7 as solid lines connecting structural templates. The structural templates are sets of atoms for which all interatomic distances are defined by chemical bonding arguments. With the exception of templates without hydrogens, OH templates, and the dummy "lysine ethyl", NMR-defined distance constraints (Table II) link every structural template defined in Figure 7 to at least one other template. The distribution of the NOE's is summarized in Figure 8. The height of each peak in Figure 8 is proportional to the number of NMR distance constraints linking the templates indexed by peak position. The figure is marked off in a grid with each block identified by its structural origin (Figures 1 and 7). Peptide bond templates are indexed by template number.

When NMR distance constraints are correlated, as they are in this example, they do not merely introduce added "bonds" into the structure but rather introduce NMR-defined structural templates.[24] These are sets of atoms for which all interatomic

(20) Hawkes, G. E.; Randall, E. W.; Hull, W. E.; Convert, O. *Biopolymers* **1980**, *19*, 1815.
(21) Wagner, G.; Pardi, A.; Wuthrich, K. *J. Am. Chem. Soc.* **1983**, *105*, 5948–5949.
(22) Following the completion of the ^{15}N NMR study, a similar study of the complex formed between Ac-D-Ala-D-Ala and vancomycin was reported by: Hawkes, G. E.; Molinari, H.; Singu, S.; Lian, L.-Y. *J. Magn. Reson.* **1987**, *74*, 188–192.
(23) Fesik, S. W.; Bolis, G.; Sham, H. L.; Olejniczak, E. T. *Biochemistry* **1987**, *26*, 1851–1859.

Table II. NOE Distances in Aridicin Aglycon–Tripeptide and –Pentapeptide Complexes

proton pairs	NOE distances: tripeptide complex	NOE distances: pentapeptide complex	bounds[d]: upper	bounds[d]: lower	proton pairs	NOE distances: tripeptide complex	NOE distances: pentapeptide complex	bounds[d]: upper	bounds[d]: lower
					(a) Aglycon Nucleus				
G1′, G2	3.8	3.7	4.4	3.4	F1′, F6	3.45	3.4	3.75	3.2
G1′, G5	3.7	3.4	4.3	3.3	F1′, BNH	3.42	3.34	3.72	3.17
G1′, G6	2.54	2.6	2.79	2.29	F1′, B2	3.49	3.69	3.79	3.24
G1′, CNH	2.87		3.12	2.62	F6, BNH	2.7	2.71	2.95	2.45
G1′, C6	3.37	3.36	3.67	3.12	F6, B2		3.59	4.19	3.19
G1′, FNH	3.75	3.62	4.35	3.35	BNH, B2	2.66	2.7	2.91	2.41
G1′, F6	3.8	4.2	4.4	3.4	B1′, B2	3.08	2.77	3.38	2.83
G1′, NMe	3.12	2.95	3.42	2.87[a]	B1′, B6	3.02	2.99	3.32	2.77
G2, CNH	3.73	3.78	4.33	3.33	B1′, ENH	2.47	2.38	2.72	2.22
G2, C2′	3.8	3.78	4.4	3.4	B1′, E6	3.73	3.44	4.33	3.33
G2, FNH	3.33	3.31	3.63	3.08	B6, ENH	3.04	2.82	3.34	2.79
G2, F1′	3.56		4.16	3.16	B6, E2	3.95	3.35	4.55	3.55
G2, F6	2.54	2.8	2.79	2.29	B6, E6		3.92	4.52	3.52
G2, BNH	3.7	3.7	4.3	3.3	B6, E1′		3.32	3.62	3.05
G5, F6		3.8	4.4	3.4	B6, A2′		3.69	4.29	3.29
G5, NME	4.31		4.54	3.54	B6, A2	3.93	3.45	4.53	3.53
G6, CNH	3.64	3.95	4.24	3.24	B6, A6	3.92	3.84	4.52	3.52
G6, NME	3.19	3.35	3.49	2.94	ENH, E1′	2.8	3.18	3.48	2.93
CNH, C2′	3.27	3.49	3.57	3.02	ENH, E6	2.76	3.01	3.01	2.51
CNH, C5	3.51	3.47	4.11	3.11	E1′, DNH	3.4	2.89	3.14	2.64[b]
CNH, C6	2.67	2.88	2.92	2.42	E1′, E2	2.47	2.6	2.72	2.22
CNH, FNH	2.70	3.04	2.95	2.45	E1′, E6		3.74	4.34	3.34
CNH, F6	3.19	3.32	3.49	2.94	E1′, A2′	3.0	2.75	3.0	2.0[b]
CNH, BNH	3.46	3.46	3.76	3.21	E1′, A2		2.88	3.13	2.63
CNH, NME	4.2	4.0	4.44	3.44	E1′, A6		3.84	4.44	3.44
C2′, C1′	2.39	2.30	2.64	2.14	E1′, A1′		3.17	3.47	2.5
C2′, C2	3.19	3.0	3.49	2.94	E2, A2′	2.48	2.7	2.73	2.23
C2′, C6	3.63	3.77	4.23	3.23	E2, A1′	3.79	3.33	4.39	3.39
C2′, FNH	3.79	3.75	4.39	3.39	E2, A2	3.52	3.31	4.12	3.12
C1′, C2	2.32	2.43	2.57	2.07	E2, DNH	2.60	2.73	2.85	2.35
C1′, C6	3.75	3.58	4.35	3.35	ANH, A6	2.62	2.57	2.87	2.37
C2, F1′	3.68	4.25	4.28	3.28	A2′, A1′	3.0	2.96	3.3	2.0[b]
C2, B2	3.54	3.77	4.14	3.14	A2′, A2	3.53	2.76	3.01	2.51
C5, B2	3.28	3.65	3.58	3.03	A2′, DNH	2.45	2.7	2.7	2.2
C6, FNH	3.53	3.56	4.13	3.13	A2′, A6		3.79	4.39	3.39
C6, B2	3.96		4.56	3.56	A1′, A2	2.68	2.54	2.93	2.43
FNH, F1′	3.2	3.23	3.5	2.95	A1′, A6	3.76	3.51	4.36	3.36
FNH, F6	2.46	2.6	2.71	2.21	A1′, DNH	3.05	3.07	3.35	2.8
FNH, BNH	2.62	2.75	2.87	2.37	A2, DNH	3.17	3.13	3.47	2.92
FNH, B2	3.13	3.34	3.43	2.88	D1′, D2		3.39	3.69	3.14
					(b) Interpeptide				
G1′, Ala^5 C$^\alpha$	3.77	3.56	4.37	3.37	A2′, Lys^3 NH		3.49	3.79	3.24
G5, Ala^5 C$^\alpha$	3.42	3.27	3.72	3.17	A1′, Lys^3 NH	3.1	3.36	3.66	3.11
G5, Ala^4 C$^\beta$		3.47	3.77	3.22[a]	A2, Lys^3 NH	3.38	3.2	3.6	2.95
G5, Ala^5 NH		3.95	4.55	3.55	DNH, Lys^3 NH	3.56	3.83	4.43	3.43
G6, Ala^5 C$^\alpha$	2.95	2.9	3.2	2.7	A1′, Lys^3 NHCOCH$_3$	2.97		3.22	2.721[a,c]
CNH, Ala^5 C$^\beta$		3.66	4.26	3.26	A1′, Ala^4 C$^\alpha$	3.33		3.63	3.08
C5, Ala^5 C$^\beta$	2.84	2.97	3.09	2.59[a]	A1′, Gln^2 C$^\gamma$ (*S*)		3.79	4.39	3.39
C6, Ala^5 C$^\beta$	3.85	3.49	4.11	3.11	A1′, Gln^2 C$^\gamma$ (*R*)		4.01	4.61	3.61
FNH, Ala^5 NH		3.93	4.53	3.53	A2, Gln^2 C$^\beta$ (*S*)		3.95	4.55	3.55
F6, Ala^5 NH		3.89	4.49	3.49	A2, Gln^2 C$^\gamma$ (*R*)		4.2	5.0	3.4
BNH, Ala^5 C$^\beta$	4.04		4.29	3.29[a]	A2, Gln^2 C$^\gamma$ (*S*)		3.59	4.19	3.19
BNH, Ala^5 NH	3.08	3.18	3.38	2.83	DNH, Ala^4 C$^\beta$	3.69	3.76	4.29	3.29[a]
B2, Ala^5 NH		3.85	4.45	3.45	DNH, Lys^3 C$^\beta$ (*S*)		3.79	4.39	3.39
B2, Ala^5 C$^\beta$	3.49	3.88	3.79	3.24[a]	DNH, Lys^3 C$^\gamma$ (*R*, *S*)		3.9	6.3	3.5
E2, Ala^4 C$^\alpha$	3.6		4.2	3.2	D2, Lys^3 C$^\beta$ (*R*)	3.34	3.6	4.2	3.2
E2, Ala^4 C$^\beta$	2.77	3.0	3.02	2.52[a]	D2, Lys^3 C$^\beta$ (*S*)	3.34	3.8	4.4	3.4
E2, Lys^3 C$^\beta$ (*R*)	3.12	3.74	4.34	3.34	D2, Lys^3 C$^\delta$ (*R*,*S*)		4.00	6.40	3.6
E2, Lys^3 NH	3.43	3.44	3.74	3.19	D4, Ala^4 C$^\beta$		3.74	4.50	4.34
					(c) Intrapeptide				
Ala^5 C$^\alpha$1, Ala^5 C$^\beta$	2.78	3.00	3.03	2.53	Lys^3 NH, Gln^2 C$^\gamma$ (*R*)		3.18	3.48	2.93
Ala^5 C$^\alpha$, Ala^5 NH	3.19	3.18	3.49	2.94	Lys^3 NH, Gln^2 C$^\gamma$ (*S*)		3.26	3.56	3.01
Ala^5 NH, Ala^4 C$^\alpha$	2.77	2.74	3.02	2.52	Lys^3 ϵ-NH, Lys^3 C$^\delta$ (*R*,*S*)		3.27	3.37	3.02
Ala^5 NH, Ala^5 C$^\beta$	3.49	3.49	3.79	3.24	Lys^3 ϵ-NH, Lys^3 NHCOCH$_3$		3.88	4.48	3.48
Ala^4 C$^\alpha$, Ala^4 NH	3.0	3.51	3.3	2.70	Gln^2 NH, Ala^1 C$^\alpha$		2.9	3.15	2.65
Ala^4 C$^\alpha$, Ala^4 C$^\beta$	2.88	2.97	3.13	2.63[a]	Gln^2 NH, Gln^2 C$^\alpha$		3.29	3.59	3.04
Ala^4 NH, Ala^4 C$^\beta$	3.4	3.33	3.7	3.15	Gln^2 NH, Gln^2 C$^\beta$ (*R*)		3.37	3.77	3.12
Ala^4 NH, Lys^3 C$^\alpha$	2.49	2.54	2.74	2.24	Gln^2 NH, Gln^2 C$^\gamma$ (*R*)		3.84	4.44	3.44
Ala^4 NH, Lys^3 C$^\beta$ (*R*)	3.0	3.19	3.49	2.94	Gln^2 NH, Gln^2 C$^\gamma$ (*S*)		3.95	4.55	3.55
Ala^4 NH, Lys^3 C$^\beta$ (*S*)	3.4	3.74	4.34	3.34	Gln^2 NH, Ala^1 C$^\beta$		4.1	4.9	3.5
Ala^4 NH, Lys^3 NH		3.94	4.54	3.54	Gln^2 NH$_2$, Gln^2 C$^\alpha$		3.87	4.47	3.47
Lys^3 C$^\alpha$, Lys^3 NH	3.62	3.3	4.22	3.22	Gln^2 C$^\alpha$, Gln^2 C$^\beta$ (*S*)		3.64	4.24	3.24
Lys^3 C$^\alpha$, Lys^3 C$^\beta$ (*R*)	3.3	3.32	3.6	3.05	Gln^2 C$^\alpha$, Gln^2 C$^\gamma$ (*S*)		3.74	4.34	3.34
Lys^3 C$^\alpha$, Lys^3 C$^\beta$ (*S*)	3.3	3.47	3.6	3.05	Ala^1 C$^\alpha$, Ala^1 C$^\beta$		3.46	3.76	3.21
Lys^3 C$^\alpha$, Lys^3 C$^\delta$		3.67	3.67	3.27	Ala^1 NH, Ala^1 C$^\beta$		3.49	3.79	3.24
Lys^3 NH, Lys^3 C$^\beta$ (*S*)	3.22	3.31	3.62	2.62	Ala^1 NH, Ala^1 NHCOCH$_3$		3.29	3.59	3.02
Lys^3 NH, Lys^3 C$^\gamma$ (*R*,*S*)	3.22	3.13	3.62	2.62	Ala^1 NH, Ala^1 C$^\beta$		3.56	4.16	3.16

Table II (Continued)

proton pairs	NOE distances: tripeptide complex	NOE distances: pentapeptide complex	bounds[d]: upper	bounds[d]: lower	proton pairs	NOE distances: tripeptide complex	NOE distances: pentapeptide complex	bounds[d]: upper	bounds[d]: lower
Extraneous Constraints Based on Chemical Shifts									
CNH, Ala^5 CO		2.1	1.5 carboxyl		FNH, Ala^5 CO		2.1	1.5 carboxyl	

[a] Distances involving these groups were computed to the centroid. [b] The signals were partially obscured. [c] The distance in the pentapeptide complex refers to the Al′, Lys^3 NH. [d] Upper and lower bounds were picked as follows: for distances less than 3 Å, bounds = $d \pm 0.25$ Å; for distances between 3 and 3.5 Å, upper bounds = $d + 0.3$ Å, lower bounds = $d - 0.25$ Å; for distances above 3.5 Å, upper bounds = $d + 0.6$ Å, lower bounds = $d - 0.4$ Å.

Table III. ^{15}N Chemical Shifts[a]

label	tripeptide: free	tripeptide: bound	tripeptide: difference	pentapeptide: free	pentapeptide: bound	pentapeptide: difference
CNH	108.0	111.7	3.7	108.0	111.7	+3.7
FNH	118.1	122.5	+4.4	118.4	122.6	+4.2
BNH	118.3	116.0	−2.3	118.1	115.9	−2.2
ENH	122.1	123.9	+1.6	122.1	123.8	+1.7
ANH	105.6	105.6	0	105.6	105.0	−0.6
DNH	128.3	128.3	0	126.5	126.8	+0.3

[a] Chemical shift reference is liquid ammonia assuming a nitromethane shift of 380.23 ppm. The correction for the bulk susceptibility difference between neat nitromethane and the DMSO-d_6–H_2O mixture was estimated to be −1.29 ppm.

Table IV. Comparison of Changes in Amide Shifts upon Complexation of Aridicin Aglycon with the Tripeptide (**2**)[a]

assgnt	chemical shifts ($\Delta\delta$): exptl (^{1}H)	chemical shifts ($\Delta\delta$): calc (^{1}H)	chemical shifts ($\Delta\delta$): ^{15}N	distance ($R_H \cdots O{=}C$), Å
N_C	4.02	3.87	3.7	1.46
N_B	1.66	2.13	−2.3	1.64
N_F	1.46	1.41	4.4	1.73
N_{Ala^5}	−0.4	−0.92		2.41
N_D	0.0	−0.89	0.0	2.39

[a] The equation used for calculating the changes in chemical shift was taken from: Wagner, G., et al. *J. Am. Chem. Soc.* **1983**, *105*, 5949.

distances are fixed by chemical bonding arguments and/or NMR-derived distances. An analyses of how the NMR-derived distance constraints are correlated is discussed in detail in ref 24. This analysis reveals *where* the conformation of the complex is "fixed" by correlated NOEs. The results of the analysis indicate that the distance constraints imposed by NOE observations need not be precise to define conformation when the observations are correlated. The analysis predicts that the GFCB region of the molecular complex will be more highly conserved in solution conformation models than is the BEAD region. This is observed in the distance geometry study and documented in greater detail in ref 24. It predicts that conformers generated by distance geometry will differ in the relationship of the GCF to the EAD regions of the aglycon. This conformational variation is observed and discussed below.

A pairwise least-squares fitting study of all atoms of the aglycon excluding hydrogens (134 atoms) indicates that all seven conformers generated are the same to within an rms deviation of 0.6 Å and that conformers b, d, and g are the same to within an rms deviation of 0.2 Å. A pairwise least-squares rms fit of the GFCB residues of the aglycon (without hydrogens) demonstrates that this region of the molecule is the same to within an rms fit of 0.2 Å for all of the conformers generated in the distance geometry study with the exception of conformer e, the conformer which is characterized by a somewhat larger distance constraint error function than the other conformers (see the Experimental Section). A pairwise least-squares rms fit restricted to the BEA residues demonstrates that the conformation of these residues is the same to within an rms deviation of 0.2 Å for all conformers generated in the distance geometry study with the exception of e and, of course, conformer f, which has a chirality error at the β-carbon of residue A.

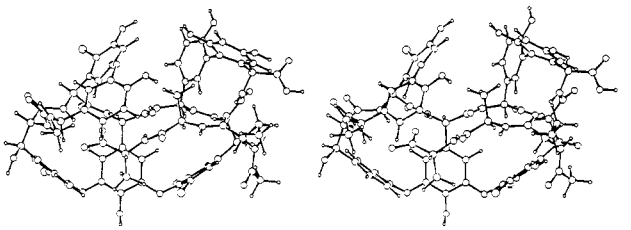

Figure 9. Solution conformation model for aridicin A aglycon bound to tripeptide (lysine side chain is truncated at the β-carbon in this diagram).

Table V. Comparison of Deviations from NOE Distance Constraints for Conformer b and Its Energy-Minimized Version

constraints, Å: upper	constraints, Å: lower	atom identifiers	deviation,[a] Å: b	deviation,[a] Å: b_{min}
4.30	3.30	G1′, G5	0.251	0.378
4.35	3.35	G1′, FNH	0.326	0.000
4.38	3.38	G1′, F6	0.145	0.000
3.63	3.08	G2, FNH	0.149	0.000
4.16	3.16	G2, F1′	0.542	0.547
4.30	3.30	G2, BHN	0.255	0.336
3.76	3.21	CHN, BHN	0.316	0.501
3.49	2.94	C2′, C2	0.167	0.581
4.23	3.23	C2′, C6	0.113	0.081
4.28	3.28	C2, F1′	0.082	0.239
3.79	3.24	F1′, B2	0.366	0.518
4.33	3.33	B1′, E6	0.124	0.105
4.55	3.35	B6, E2	0.218	0.240
4.12	3.12	E2, A2	0.196	0.190
3.47	2.92	A2, DHN	0.164	0.303
		error[b]	1.543	2.052

[a] Greater than 0.05 Å. [b] The square root of the distance constraint error function defined in eq 1 evaluated over all distance constraints.

Molecular graphics comparisons confirmed that five essentially identical conformers (a–d, g) were generated in the distance geometry study along with a somewhat different and more strained conformer e. Conformer e has a larger error function value than does conformer b (see the Experimental Section).

The correlation of the NMR distance constraints in this data set predicts that conformational domains associated with the GCFB and BEAD residues for this data set are connected at the B residue. This becomes intuitively reasonable from an inspection of the data presented in Figure 8 of ref 24. Distance geometry conformers b and e were subjected to energy refinement using Gaustiger charges and MAXIMIN force field parameters.[25] Energy refinement maximizes the hydrogen-bonding interactions between the aglycon and bound peptide while minimizing steric and other strain in the molecule. The energies of the minimized versions of conformers b and e were 73.7 and 86.1 kcal, respectively. On the basis of visual assessment, conformer e on minimization becomes a higher energy strained version of conformer b.

The minimized version of conformer b (Figure 9) is incorporated into the solution conformation models of the molecular complexes of the aglycon of aridicin A discussed in greater detail below.

(24) (a) Hempel, J. C.; Mueller, L.; Heald, S. L.; Jeffs, P. W. *Proceedings of the 10th American Peptide Symposium*; Marshall, G. R., Ed.; ESCOM Science Publishers B.V.: The Netherlands, 1988; pp 62–64. (b) Hempel, J. C. *J. Am. Chem. Soc.*, preceding paper in this issue.

(25) Sybyl, version 3.4, Registered Trademark, Tripos Associates, Clayton, MO.

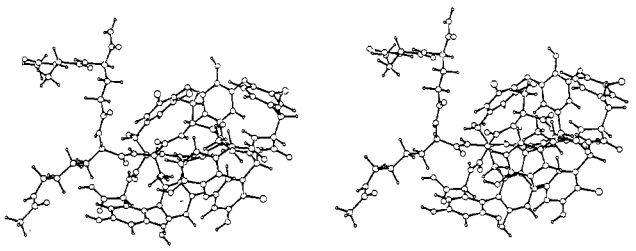

Figure 10. Solution conformation model for aridicin A aglycon bound to pentapeptide (**3**). The conformation of the lysine side chain past the γ-carbon is not defined by distance constraints.

Deviations from the distance constraints used to define this model in the distance geometry study are compared in Table V for conformer b and the minimized version of conformer b. NOE deviations greater than 0.05 Å are without exception associated with distances longer than the upper bound of an NOE. Most of the distance bound violations occur in the GCF region of the molecule even though the GCFB region is the most conserved region in modeling studies. This may be due to the effects of spin diffusion that are not incorporated into the asymmetric bounds or may reflect the effects of conformational variation in this region, leading to the definition of a single set of constraints derived from two or more similar conformers. Since the experimentally determined distance constraints that define the molecular conformation of the core of the molecular complexes of the aglycon with the tri- and pentapeptide are the same, any effects of the full side chains on the conformation of the complex as a whole are included in this model. Similarly, the model reflects the effect of solvent on the conformation of the complex even though solvent is not specifically considered in the generation of the model.

The solution conformation of the complex of the aglycon–pentapeptide complex was derived from consideration of the distance constraints provided by the NOESY data for the Lys and γ-Gln side chains. Both inter- and intrapeptide NOE's were utilized to define the orientation of the lysine and γ-glutamine side chains relative to the aglycon nucleus. This was accomplished by holding the core of the molecular complex fixed and then utilizing the inter- and intrapeptide NOE-derived distances between the aglycon and the Lys-γ-Gln-L-^{1}Ala residues in a series of interactive modeling operations by employing the graphics capability of the Evans and Sutherland PS-390. The structure derived is consistent with the distance bounds provided by the NOE data, but the possibility of other arrangements of the side chains cannot be excluded. The increased motional characteristics in the terminal L-Ala^5 residue and the C^γ–C^ϵ side chain of the lysine atoms are such that in these regions the structure depicted in Figure 10 is one representative of many conformational states. A further reflection of the good agreement of the energy-minimized version of conformer b of the pentapeptide complex derived from the distance geometry is the correlation of the experimental values with the calculated values of the NH–CH^α dihedral angles obtained from J coupling constants (Table VI).

NMR studies have also been reported for two closely related structures, the aglycon of aridicin in solution[4d] and the molecular complex of a pseudo-aglycon of ristocetin bound to the tripeptide Ac_2-Lys-D-Ala-D-Ala.[6] The 40 NOE observations reported previously[4d] for the aglycon of aridicin A in solution present a subset of the data presented in Table II. The 17 NMR observations previously tabulated[6] for the region of the ristocetin complex common to the aridicin A aglycon complex are also a subset of Table II.[26] Although substitution patterns of the aromatic side chains of aridicin A and ristocetin differ, the structural template analysis given in Figure 7 is the same. The solution conformation model reported here is therefore also one of the acceptable solution conformation models for uncomplexed aridicin A aglycon and, within the criteria of the 17 NOE's previously tabulated[6] for the ristocetin complex, for the common region of the ristocetin complex as well.

Table VI. Compariosn of Dihedral Angles Derived[a] from J Couplings and the Model

	calc θ,[b] deg	measd θ from computer model, deg
J(CNH, C2′)	180	176
J(FNH, F1′)	164	180
J(BNH, B1′)	−157	−178
J(ANH, A2′)	163	164
J(DNH, D1′)	−146	−147
J(Ala^5 NH, Ala^5 C^α)	−150	−171
J(Ala^4 NH, Ala^4 C^α)	−142	−122
J(Lys^3 NH, Lys^3 C^α)	−137	−163

[a] Calculated from the equation of: Kopple, Wiley, and Tauke, *Biopolymers* **1973**, *12*, 627–636. [b] The signs were established from the solution conformation model derived with distance geometry. Dihedral constraints calculated from J couplings were not included as distance constraints in the modeling study.

Two regions of the solution conformation model are of particular interest in this regard. We note that the conformation of the F ring relative to the G ring is not fixed by direct distance constraints (Table II and Figure 8). The solution conformation model proposed here differs from the conformation previously proposed for aridicin A aglycon in solution in the sense of the "twist" of the G and F rings. However, the two conformers are equally acceptable models for the aglycon in solution since this orientation is not defined by distance constraints in the NMR data set for the uncomplexed aglycon. Conformational variation has been predicted for the orientation of the F side chain in the ristocetin complex on the basis of molecular dynamics simulations of the complex.[6] Our data do not rule out the possibility of conformational variability in this region but are consistent with the conformations proposed in Figures 9 and 10, taking into account the effects of spin diffusion in this region of the molecule. A more complete discussion of this region of the molecule is provided in ref 24. It is interesting to note, by contrast, that the relative conformations of the D and E rings are fixed by the distance constraints in all three NMR data sets. The relative orientation of D and E rings defined by the NMR studies also fits the CDP1 crystal structure.[5]

Summary

The models generated for the complexes of aridicin aglycon containing the tripeptide (**2**) or pentapeptide (**3**) derived in this study are consistent with the general structural features described previously for the complexes of **2** with ristocetin,[27] avoparcin,[16c] and vancomycin.[28] These features include (i) a hydrophobic cavity in the aglycon containing three parallel-oriented NH groups that form hydrogen bonds to the C-terminal alanine carboxylate in the bound peptide and (ii) a hydrogen bond between Ala^4 NH and the B-2′ carbonyl. However, contrary to earlier studies,[28] our results from both ^{1}H and ^{15}N chemical shift comparisons fail to indicate the existence of a hydrogen bond between the Lys^3 carbonyl and DNH as has been previously proposed for the tripeptide complexes of vancomycin and ristocetin. The disposition of the L-lysine side chain in the complexes of both **2** and **3** is found to lie over the face of ring D. This is in agreement with results reported for aqueous solutions of the complexes between **2** and ristocetin[27] and avoparcin,[16c] respectively. The intrapeptide NOE's and the NH–C^αH coupling constant values of the bound forms of tripeptide (**2**) and pentapeptide (**3**) indicate that the backbone conformation of the L-Lys and the D-Ala residues is extended. While there is evidence for increased motion in the backbone and side-chain atoms of the L-Lys, L-Gln, and L-Ala^1 residues of the pentapeptide when compared to the C-terminal D-Ala^5 and D-Ala^4

(26) With the caveat that it is not possible to completely resolve the nomenclature in the A ring of the two studies from the data tabulated in ref 6. Both A2 and A6 are assigned in the current study whereas only one of these protons was assigned in ref 6.

(27) Williamson, M. P.; Williams, D. H. *J. Chem. Soc., Perkin Trans. 1*, **1985**, 949–956.

(28) Williams, D. H.; Williamson, M. P.; Butcher, D. W.; Hammond, S. J. *J. Am. Chem. Soc.* **1983**, *105*, 1332–1339.

groups, the NOE data indicate certain conformational preferences for the Lys and Gln side chains in the complex as depicted in Figure 5. The additional hydrophobic interactions associated with the Gln side chain and the aridicin core suggested by this NMR data, in conjunction with entropic effects associated with desolvation of the L-Ala[1] and L-α-Gln, may be important in accounting for the increased lifetime of the pentapeptide complex compared to the tripeptide complex.

Utilization of accurate volume integrals from the NOESY spectra obtained at two mixing times to derive $^1H-^1H$ distance information obviously has limitations in that the effects of spin diffusion are neglected. However the use of asymmetric distance bounds to compensate for the effects of spin diffusion proved successful in that six of the seven structures obtained by the use of a distance geometry algorithm showed a high degree of convergence, reflecting the correlation of the NMR distance constraints. On the basis of these results, we feel confident that, for structures that are comparable in their rigidity to aridicin aglycon, this method is capable of providing well-built model structures. Although it is less rigorous than procedures to monitor build-up rates that were used for a similar compound by Fesik and workers,[6] it has advantages in that while it is much simpler, it is capable of providing structural models of similar quality. An assessment of the validity of this latter statement may be obtained from a comparison of the distance information from this study and that reported by Fesik et al.[6] for the core region of ristocetin. Of the 17 NOE constraints that are tabulated for the core region of the complex of ristocetin aglycon and the tripeptide (**2**), only two fall outside the distance bounds derived for the aridicin aglycon complexes in the current study.[26] These deviations involve the interpeptide NOE's linking D-Ala[4] to G1′ and to E2. The values derived for the ristocetin complex are 0.3 and 0.5 Å longer than the upper bounds assigned for the aridicin A complex in this study.

The NMR data support the proposal of a single solution conformation of the aglycon irrespective of whether it is bound to the tripeptide (**2**) or the pentapeptide (**3**) and suggest that both **2** and **3** are good models for probing the binding interactions at the molecular level of this class of antibiotics to bacterial cell-wall intermediates.

The results of the current study, when used in conjunction with the analysis of the NMR constraints described in ref 24, make it possible to designate those regions of the structure that are well-defined by the distance information and also to make some predictions about regions that may be exhibiting more mobility or conformational diversity. We believe that the NMR methods described will be generally useful for obtaining well-built models of structures that do not contain structural regions exhibiting grossly different time scales of internal motion.

Studies of Rare-Earth Stannates by ^{119}Sn MAS NMR. The Use of Paramagnetic Shift Probes in the Solid State

Clare P. Grey,[†] Christopher M. Dobson,*[,‡] Anthony K. Cheetham,[†] and Roger J. B. Jakeman[†]

Contribution from the Chemical Crystallography Laboratory, University of Oxford, 9 Parks Road, Oxford OX1 3PD, U.K., and the Inorganic Chemistry Laboratory, University of Oxford, South Parks Road, Oxford OX1 3QR, U.K. *Received June 20, 1988*

Abstract: ^{119}Sn MAS NMR spectra have been obtained from members of a series of rare-earth stannates $Ln_2Sn_2O_7$ (Ln = La, Pr, Nd, Sm, Eu, Tm, Yb, Lu, and Y), all of which adopt the pyrochlore structure. Apart from $La_2Sn_2O_7$, $Lu_2Sn_2O_7$, and $Y_2Sn_2O_7$, these compounds are paramagnetic and exhibit a very large variation in ^{119}Sn chemical shifts (from approximately +5400 to −4200 ppm), which can be attributed principally to a Fermi contact shift mechanism. The spectra from the paramagnetic samples have large overall line widths associated with the substantial anisotropy of the shift, but the individual peaks within the spinning sideband manifolds remain sharp. Several tin pyrochlore solid solutions have also been studied (namely $Y_{2-y}Ln_ySn_2O_7$ where Ln = Sm, Nd, Pr, and Eu and $La_{2-y}Nd_ySn_2O_7$) by ^{119}Sn MAS NMR. When the short relaxation times of nuclei close to paramagnetic centers were exploited, a series of peaks were observed, associated with the substitution of paramagnetic for diamagnetic lanthanide ions in the local coordination around a tin atom. For $Y_{2-y}Sm_ySn_2O_7$ the composition of the solid solution could be determined from the intensities of these peaks. In the solid solutions the ^{119}Sn nuclei were found to be sensitive not only to neighboring paramagnetic ions but also to paramagnetic ions in the second and third coordination spheres. The shifts induced in these cases arise primarily from a through-space dipolar "pseudocontact" mechanism and can be interpreted with a model for the site symmetry based on the crystal structure.

Despite extensive exploitation of the paramagnetic properties of metal complexes[1,2] in NMR studies of molecules in solution, very few NMR experiments on such compounds in the solid state have been carried out. One reason for this is that it is often difficult to observe well-resolved NMR signals from paramagnetic solids, either because relaxation induced by the magnetic moments of unpaired electrons results in substantial line broadening or because large anisotropic interactions present in a solid (usually averaged by rapid molecular motion in solution) cause a large dispersion of the chemical shift in a powder sample. The lanthanides, however, form an important class of paramagnetic ions in this context because, with the exception of gadolinium, their electron relaxation (T_{1e}) times are sufficiently short for the nucleus to be coupled only weakly to the electronic spin system and relatively sharp resonances can be observed. Recently, ^{13}C NMR spectra of lanthanide acetates[3,4] have demonstrated that high-

[†] Chemical Crystallography Laboratory.
[‡] Inorganic Chemistry Laboratory.

(1) Hinckley, C. C. *J. Am. Chem. Soc.* **1969**, *91*, 5160-5162.
(2) Dobson, C. M.; Levine, B. A. *New Techniques in Biophysics and Cell Biology*; Pain, R. H., Smith, B. J., Eds.; Wiley-Interscience: New York, 1976; Vol. 3, pp 19-90.
(3) Chacko, V. P.; Ganapathy, S.; Bryant, R. G. *J. Am. Chem. Soc.* **1983**, *105*, 5491-5492. Ganapathy, S.; Chacko, V. P.; Bryant, R. G.; Etter, M. C. *J. Am. Chem. Soc.* **1986**, *108*, 3159-3165.
(4) Campell, G. C.; Crosby, R. C.; Haw, J. F. *J. Magn. Reson.* **1986**, *69*, 191-195.

0002-7863/89/1511-0505$01.50/0